DEGRADATION OF ADHESION STRENGTH WITHIN MINI-MODULES DURING DAMP-HEAT EXPOSURE

Dan Wu*, Jiang Zhu, Thomas R. Betts, Ralph Gottschalg
Centre for Renewable Energy Systems Technology (CREST),
School of Electronic, Electrical and Systems Engineering,
Loughborough University, LE11 3TU, United Kingdom
*Tel: +44(0)1509 635318, Fax: +44 (0)1509 635301, E-mail: D.Wu@lboro.ac.uk

ABSTRACT: The degradation of adhesion strength between back-sheet and encapsulant due to moisture ingress was investigated for commercial crystalline silicon photovoltaic (PV) mini-modules. The damp-heat test originated from qualification test was carried out at five different temperature and humidity conditions (95°C/85% RH, 85°C/85% RH, 65°C/85% RH, 85°C/65% RH and 85°C/45% RH) to assess the impact of stress levels on test outcomes. The adhesion strength was measured by 90° peel tests, carried out at specified degradation intervals. Several visual defects were observed, including delamination, moisture ingress and bubble formation. The adhesion strength showed a stretched exponential decay with time and significant influences of test conditions was demonstrated. A humidity dose model was proposed by assuming micro-climates seen by the modules, i.e. surface relative humidity of the back-sheet as the driving factor for an Arrhenius based model using temperature as accelerating factor. The correlation between adhesion degradation and humidity dose was investigated and an exponential model was developed to represent this correlation with extracted activation energy (E_a) of 63kJ/mol. This supplies a potential model for the estimation of adhesion strength decay triggered out by humidity in dependence of the humidity conditions.
Keywords: adhesion strength, peel test, damp heat, adhesion degradation modelling

1 INTRODUCTION

Good encapsulation is required for photovoltaic (PV) modules to ensure reliability and lifetime. The active PV material is usually encapsulated by front cover, polymeric encapsulant, back sheet, and edge seal [1]. The different components are bonded adhesively to each other. This forms a multilayer system which ensures the safety and to some extent the performance of the module but also results many interfaces. These interfaces are potential paths for contaminant ingress as well as leakage current and thus potential sources for arcing [2]. Delamination can also happen in these interfaces [3-5]. Delamination can reduce the efficiency of the moisture barrier and result in further degradation mechanisms such as metallisation corrosion, polymer decomposition, light transmission losses and reduction of resistance of the encapsulant [6, 7]. The delaminated area will also suffer from reduced heat dissipation which has the potential to cause thermal fatigue and hot spotting [8].Therefore, the strength of these bonds is crucial for module reliability and is the topic of this paper. It will be shown that de-bonding of the back-sheet is happening at the interface between encapsulant and back-sheet (rather than breaking of the encapsulant), and thus the focus of this paper will be on this particular interface.

The loss of adhesion strength is expected to vary with the operating environment, i.e. depends on factors of temperature, humidity, and irradiance including UV etc. The long-term aim of this work is to model this behaviour. This requires the superposition of a number of different ageing mechanisms which may act independently or not. Each of these effects needs to be investigated in isolation before an overall model can be given. This paper concentrates on the adhesion reliability of the interface between encapsulant and back-sheet to withstand the effects of moisture penetration which is influenced by temperature. The objective is to understand the effects of sustained steady state stresses of humidity and temperature on the back-sheet adhesion. In standard qualification testing, this is carried out through the damp-heat test, where modules are exposed to a relative humidity of 85% at a temperature of 85°C [9, 10]. An underlying assumption is that the external humidity is higher than the equivalent chemical potential in the packaging, which means the direction of humidity is from environment into the packaging. Once the direction of moisture is different, i.e. the moisture within packaging is dried out into the atmosphere, a different potential failure mode will be triggered and the damp-heat test will lose its validity. Nevertheless, the focus of this paper is on the damp-heat test and how different conditions influence the loss of adhesion due to moisture ingress.

Moisture can influence the adhesion strength in several different ways. Today, ethylene vinyl acetate (EVA) is the most commonly utilised encapsulant in the PV industry. Normally, the encapsulation is carried out using sheets of EVA which contain a complex cocktail of additives except EVA resin to enhance its performance. One of the additives is adhesion promoter normally in the form of silane coupling agents which are used to enhance adhesion between EVA and glass and back-sheet by forming silicon-oxygen covalent bonds [11]. Humidity uptake in EVA will cause bond hydrolysis, which in turn leads to reduced adhesion strength. Such a de-bonding reaction is accelerated by temperature. The presence of moisture also influences intermolecular secondary forces (i.e. Van der Waals) between encapsulant and back-sheet [12]. In general, moisture ingress within polymer is accelerated by temperature [13, 14]. Under this context, for the damp-heat test, an assumption can be made that the loss of adhesion strength is primarily induced by moisture and temperature in itself is not a stress factor but just accelerator of the effects of humidity.

There are a number of studies of adhesion strength for PV modules. Some of them report reduced adhesion but are normally based on progressive uncontrolled ageing or carried out at a single controlled operating condition. Jorgensen and McMahon [15] measured the peel strength of different interfaces within thin film PV modules of various technologies and structures before and after damp heat conditioning, and under UV light.

Non-uniform reduction of strength was observed at different interfaces and they suggested that test at higher temperature and relative humidity levels were preferred to screen modules. At NREL, extensive peel tests were conducted to understand the factors influencing the adhesion strength of EVA to glass substrates, including EVA type and formulation, backfoil type and manufacturing source, glass type, surface cleaning methods and surface priming treatment [16]. Pern and Jorgensen [17] investigated the adhesion strength between glass and EVA and its resistance to damp heat exposure by developing different primer formulations for EVA. Enhanced adhesion strength is observed for laminates with EVA having high density siloxane primers. Although increasing concern is given to adhesion issues, there have been few reliability tests and quantitative degradation studies. The degradation pattern of adhesion strength is not established for these layers and the numerical correlation to environmental stresses such as temperature and humidity is currently largely being postulated.

This paper presents an approach that allows the measurement of degradation of adhesion strength between back-sheet and encapsulant for PV modules and develops potential modelling methods for the correlation between adhesion strength degradation with humidity and temperature. Well-controlled peel tests are used to measure the adhesion strength at certain time intervals during which devices were exposed to damp-heat in different operating conditions. As this research only focus on humidity induced degradation, no dry conditions and extremely high temperature levels are considered as these may introduce different failure mechanisms. The degradation of adhesion strength with time is assessed, and the correlation between degradation and environmental stresses of humidity and temperature is also investigated.

2 EXPERIMENTAL DESIGN

The aim of the experiment is to investigate the degradation of adhesion strength between back-sheet and encapsulant with exposure to high humidity (relative to residual humidity within the sample) and understand the acceleration of different stress levels. This requires exposure of samples to different temperature and humidity levels as well as the measurement of the adhesion strength. The exposures are typically achieved by multiple environmental chambers setting up at different conditions. The adhesion is measured with a destructive 90^{o} peel test in which samples can only be used for a single time. Multiple samples are thus required which will introduce noise and to minimise the noise, samples produced by a single manufacturer are used.

Samples used in this work are commercial frameless small area laminates with polycrystalline silicon solar cells. These laminates have no edge seal which simplify moisture absorption and accelerate the overall humidity ingress compared with laminates protected by edge seal. The laminate size is 140 mm by 100 mm in length and width. The encapsulant material is EVA and the back-sheet is double layers of polyethylene terephthalate (PET) which were verified by Fourier Transform Infrared Spectrometer (FTIR) test. The thicknesses of EVA sheet and back-sheet are approximately 400 μm and 250 μm respectively which were measured by microscope. Indoor accelerated damp-heat tests were conducted in environmental chambers at five different conditions as listed in Table 1. The testing time and number of modules at each condition are shown in Fig. 1. A number of trial tests were carried out at 85^{o}C/85%RH to roughly qualify the module and the test points were chosen according to the data collected there. It was found that the adhesion strength became 2-3N/cm after around only 100h exposure. Therefore, in general, daily measurements were carried out.

Table I: Test conditions for PV modules

T \ RH	85%	65%	45%
95^{o}C	✓		
85^{o}C	✓	✓	✓
65^{o}C	✓		

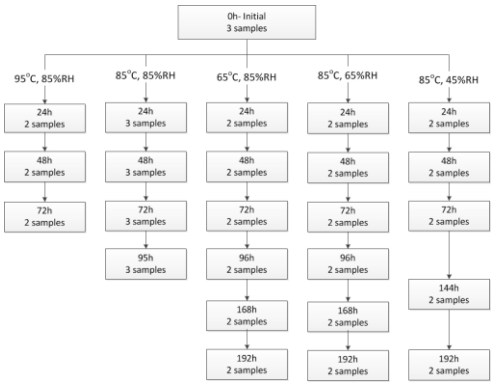

Fig. 1 Flow chart of testing time and number of samples for each degradation condition

The back-sheet of each module was cut by CO_2 laser into strips of 10mm width (i.e. ten strips along the long edge of the modules) once the intended stress level was reached. The laser cut was used as this could be done with an automated laser jet result in good controlled cutting depth and accurately placed cuts. The cutting speed was set to 762mm/s with a power of 32 W and 10 passes to achieve the desired cutting depth. Laser cut has many advantages compared with other alternative cutting methods such as blade or disc based cutting. The quality of the cuts is shown in Fig. 2, which presents an image of one of the typical strips cut measured by a coherence correlation interferometer (CCI). The left figure is the 3-D image of the surface profile near the cut while the right one is the corresponding 2-D image. The colour scale indicates the depth of the scanned surface. The trench in Fig 2(a) is the cut. A depth of 250 μm is observed, which equals to the thickness of the back-sheet (roughly 250 μm). Compared with commonly used blade cutting, laser cutting is a quick and precise cutting method with accurate control of cutting depth, ensuring little damage of the encapsulant layer and also guaranteeing parallel strips. Each of the peel strips is 10mm in width and 100mm in length. The first 15mm of each strip was disregarded because it was peeled off before testing to form a tab so that the grip of the peel test machine could be secured to hold the strip.

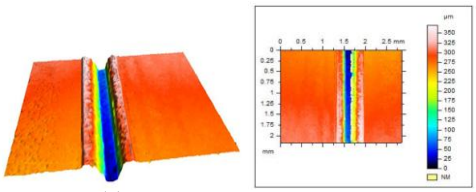

(a) (b)

Fig 2 Interferometer image of the cutting of the back-sheet

Each of the strips was then peeled off using a 90° peel test setup (Chatallion) with a crosshead speed of 50mm/min at ambient room temperature. The test was conducted based on standard BS EN ISO 8510 [18]. The peel test is very sensitive to environment, sample and testing conditions, and thus requires a large number of tests to ensure sufficient accuracy and good averaging. 20-30 strips from two to three different modules were examined on average for each condition at each measurement point (see Fig. 1). A visual inspection was also carried out after removal of the modules from the environmental chambers, prior to the laser cutting.

3 EXPERIMENTAL RESULTS

3.1 Visual inspection

Several types of defects were observed during testing. Some of the more severe ones are depicted in Fig. 3. Delamination was observed, mostly at corners and edges of the mini-module. The lack of edge seal of the module leaves the edge directly open to the environment where stronger influences were seen compared with those areas with moisture barrier. Imperfect lamination may also contribute to the developing fault. Moisture penetration into the module was also observed and bubbles appeared at the front Glass/EVA interface. After 24h ageing at 95°C/85%RH, a large bubble around the electrodes was observed. This is due to the poor protection around the external contacts where an access cut in the back-sheet is not well sealed, allowing moisture ingress. The majority of the module would have passed visual inspection.

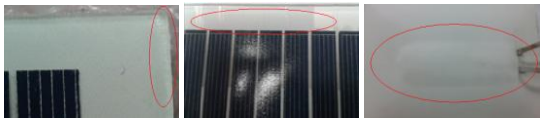

Fig. 3 Defects observed after damp heat testing: edge/corner delamination (a), moisture ingress (b) and bubble near electrode exit (c)

3.2 Peel test results

The peel test measures the fracture energy required to separate the surfaces of the interface as a function of time or the equivalent displacement. The separation can happen either at the interface or in the bulk of a material (cohesive failure) if the structural integrity is weaker than the bonding strength at the interface. This was checked visually as well as by taking microscopic photos at the surface of the inner side of back-sheet. An example is shown in Fig. 4 which presents the surface microscopic image of the peeled PET strip after 48 hours degradation at 85°C/85%RH. No EVA is seen attached on this surface which indicates that the failure mechanism is interfacial rather than cohesive and the measured adhesion strength is that of the interface of back-sheet-encapsulant.

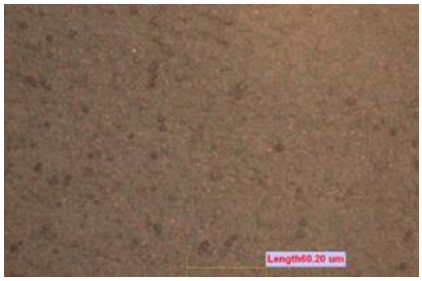

Fig. 4 Microscopic image of the surface of the inner side of back-sheet for the module exposed at 85°C/85%RH after 48h degradation (magnification x10)

A typical result of the peel test can be seen in Fig. 5. Three stages can be defined as following:

(1). Loading of the peeling arm as it takes up slack. The pull force increases until the strip is fully tensioned to the peel tip where peeling starts.

(2). Propagation of the interface separation. Data from this area gives the adhesion strength sought. In this study, the first 1cm after tensioning is discarded, as the adhesion strength is not reliably measurable in this region. Data of the last 2cm is not used either, as the silicon cell of the module ends 1cm before the edge of the module. A further 1cm at the end side is excluded to eliminate variation caused by the tolerance of the size of the silicon cell. The average value of the remaining data is used for the degradation study.

(3). Completion of the separation. A sudden drop of the peel strength to zero is characterized in this stage.

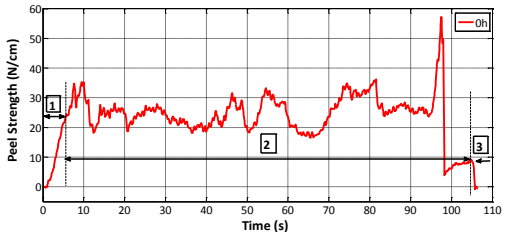

(a) Peel test data for un-aged module

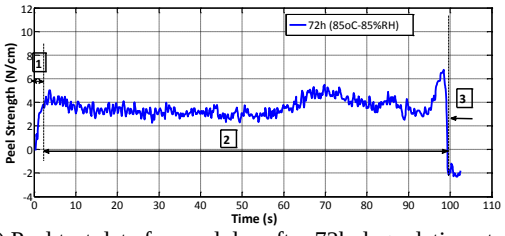

(b) Peel test data for modules after 72h degradation at 85°C/85%RH

Fig. 5 Typical peel test results

The measured peel strength is module dependent. The variation over some of the measured strips is smaller while larger for others. An example is given in Fig.5 where the top figure fluctuates significantly and the plot of the bottom figure is relatively flat. Such variations may result from several factors such as the variations in manufacturing process of the material and imperfect lamination quality due to uneven temperature and pressure distribution.

3.3 Degradation of adhesion strength with time

Adhesion strengths are plotted against stress exposure time in Fig. 6 at 95°C/85% RH, 85°C/85% RH, 65°C/85% RH, 85°C/65% RH and 85°C/45% RH. The adhesion strength under different conditions showed similar degradation pattern in the shape of a stretched exponent. The adhesion strength decreases quickly at the beginning and then tends to slow down after a certain time. The increase of humidity accelerates loss of adhesion. Temperature further enhances the effect of humidity in a larger rate. In general, the reduction of the adhesion is rather quick, but this can be attributed to the high stress levels and the absence of edge seal. The small sample size of 0.012m^2 which is about 1-2% of a normal commercial module's size further increases humidity uptake. All of these factors increase acceleration achieved in the test, which would be seen as a multiplier of the test. The principles of degradation remain unchanged, though.

The adhesion strength can be fitted by the following equation:

$$S = S_0 e^{-(\frac{t}{t_{del}})^{\beta}} \quad (1)$$

where t is the degradation time, S_0 is the adhesion strength before degradation (i.e. at t=0), S is the strength at time t, β and t_{del} are two parameters controlling the slope and tail of the degradation curves. The parameter t_{del} primarily determines the slope of the degradation and β represents the magnitude of the influence of t_{del}. The overall behaviour of the degradation depends on the combination of t_{del} and β. The fitted values of t_{del} and β for each condition can be seen from Table 2. Each condition has different values of t_{del} and β. Therefore, the predicting of the reduction of adhesion strength with time based on equation (1) needs extra modelling of the dependence of t_{del} and β on stress levels and duration. An alternative simplified solution is to find out a parameter that enables the modelling of adhesion degradation with a single variable. This will be discussed later in the paper.

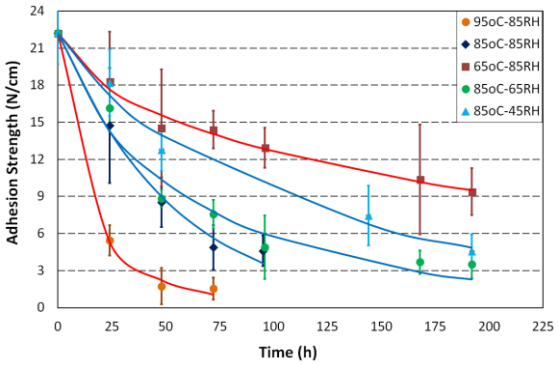

Fig. 6 Reduction of peel strength in dependence of applied stresses and time

Table ɪ: Parameters for the adhesion degradation

Conditions	t_{del}	β	Experiment R_D	Acceleration Factor
65°C-85%RH	249.8	0.63	11.08%	1
85°C-85%RH	53	1.028	25.53%	2.3
95°C-85%RH	14.3	0.687	56.20%	5.07
85°C-65%RH	67.99	0.789	20.5%	1.85
85°C-45%RH	117.9	0.857	13.93%	1.26

Also listed in Table 2 are the degradation rates (R_D) calculated from experimental data (average R_D for each condition) as well as the corresponding acceleration rates (AR). The degradation rate is defined as the percentage adhesion strength decline over time:

$$R_D = \frac{S_0 - S_t}{\Delta t} \quad (2)$$

where Δt is the time duration of exposure and S_t is the adhesion strength at the time of t. The degradation rate at 65°C/85% RH is the smallest while that at 95°C/85% RH is the highest. If taking the degradation at 65°C/85% RH as the baseline where the smallest degradation happened, 1-5 times acceleration rates (the ratio of the degradation rates at different ageing conditions) are observed for the other four conditions. Lower stress levels (lower temperature, lower humidity) will cause lower degradation up to a point. The stress levels chosen here are somewhat arbitrary based on qualification test standards but give an indication of the acceleration rates in this set of experimental ranges. Once the applied humidity is low enough, the direction of humidity flow will change from ingress into PV modules to drying out of the module, which will cause entirely different degradation effects and thus it is not possible to extrapolate the behaviour to very low humidity conditions.

3.4 Spatially distribution of adhesion strength degradation

The peel strength shown in Fig 6 is average values for the entire module at each condition. They do not give any indication of variations of adhesion strength across the module. An impression of this variation can be obtained by aligning all peel tests for one module side-by-side and create a contour plot of the spatial profile. This gives an insight of how the adhesion strength varies over the surface of a module and how it changes over time under stress. Fig. 7 is an example of the contour plots showing the development of adhesion strength at 65 ℃/85%RH with an un-aged module and three modules stressed for 24h, 72h and 192h. The x-axis represents the strip number with each strip in 10mm width and the y-axis is the distance from the peeling end in mm, i.e. the length of strips. The colour scale of the contour plots demonstrates the adhesion strength in N/cm and the blank areas at corners and edges indicate where the strips snapped during the peel.

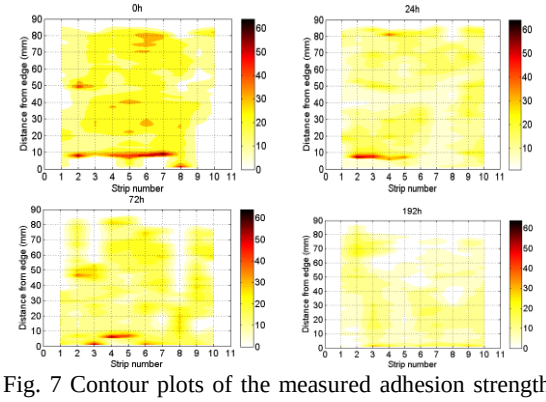

Fig. 7 Contour plots of the measured adhesion strengths over the module surface for the un-aged module (top left) and modules aged after 24h (top right), 72h (bottom left) and 192h (bottom right) at 65 ℃/ 85% RH condition (each strip is in 10mm width).

As shown in Fig. 7, the peeling of all strips started close to the distance of 85mm and ended at 0mm point. The first 15mm was peeled off before the actual test to create the peeling tab for the machine to seize. Large spikes were observed more often near 10mm because that is where the silicon cells end and although it was checked that the peeling still happened at the EVA-back-sheet interface, the sudden change of the substrate result in higher adhesion values. Before degradation, the edge of the module had lower adhesion strength than the centre. Possible explanations are the bad lamination at the edge plus the opened edge of the module is influenced by outdoor environment so that some degradation occurred. In general, the adhesion strength reduced as the modules degraded. Several more spikes existed at different locations before degradation but gradually disappeared throughout stress exposure and became more evenly distributed. Although from this contour map, it is not easy to define a precise degradation pattern, it presents the spatial distribution of adhesion strength across the surface of the whole module which is helpful for the identification of the weakest spot and to some extent the degradation mechanisms. The 24h image shows two perpendicular lines with low adhesion strength, where it appears that water 'channelled' into the mini-module. The 72h and 192h images seem to show a reduction of the adhesion strength from the inside to the outside. It looks like the water is accumulated in the centre while released in the outside enabling moisture desorption at these areas.

4 ADHESION DEGRADATION IN DEPENDENCE OF HUMIDITY AND TEMPERATURE

4.1 Stress model development

The degradation is investigated by correlating degradation rate and environmental stresses. In order to describe the stresses acting on the modules over a certain period of time, the ambient macro climate, i.e. the relative humidity measured at ambient temperature, needs to be translated into module's micro climate first, i.e. the relative humidity seen at the surface of back-sheet under module's temperature. The module's operating temperature will be elevated with respect to ambient conditions. This means that the relative humidity experienced by the device is lower than one would see from ambient. There are many different models can be used to predict module temperature from ambient temperature [19-21]. Compared with outdoor exposure, the standard damp-heat tests in environmental chambers are different in this respect because the device temperature is equal to ambient temperature, i.e. module temperature (T_m) is identical to chamber temperature (T_a). This difference needs to be considered when attempting to predict a service life-time for an outdoor installation.

The micro-climatic relative surface humidity at the back-sheet is calculated as shown in Eq(3)-(4) using the model proposed by Koehl et al [22]. This assumes that the surface of back-sheet is in thermodynamic equilibrium with the atmosphere and the temperature is uniform across the module:

$$RH_a = \frac{P_w}{P_s(T_a)} \tag{3}$$

$$RH_m = \frac{P_w}{P_s(T_m)} = \frac{RH_a \cdot P_s(T_a)}{P_s(T_m)} \tag{4}$$

where RH_a is the ambient relative humidity, P_w is the partial water vapour pressure of atmosphere, $P_s(T_a)$ and $P_s(T_m)$ are saturated water vapour pressure at ambient temperature (T_a) and module temperature (T_m) respectively. The calculations of saturated and absolute water vapour pressure are according to the standard BS 1339-1:2002 [23]:

$$P_s = f \cdot P_s' \tag{5}$$

$$P_w = RH \cdot P_s = RH \cdot f \cdot P_s' \tag{6}$$

where P_s' is the pure saturation vapour pressure at a given temperature, P_s is the saturated vapour pressure in the air, f is an enhancement factor to transfer P_s' to P_s, and P_w is the partial pressure of water vapour in the air. As both P_s' and f are functions of temperature, P_s and P_w are also dependent on temperature. Fig. 8 shows the actual water vapour pressure (P_w) curve versus temperature at different RH levels from 45% to 100%. The relationship is straightforward to calculate but introduces an exponential relationship between water vapour pressure and temperature. An outdoor environment condition of 45%RH and 35°C will result in an ambient water vapour pressure of 2.5KPa. But at the same relative humidity level with a higher temperature of 85°C used in this study, the water vapour pressure will increase to 26.2KPa which is almost 10 times of that in outdoor condition. Similarly, if assuming the module temperature of an outdoor installed PV module can reach to 85°C, the saturated water vapour pressure at the back-sheet surface can be much higher than that at ambient temperature. Therefore, the differences between ambient relative humidity and module relative humidity induced by differences between T_a and T_m need to be considered when describing the stresses experienced by the module.

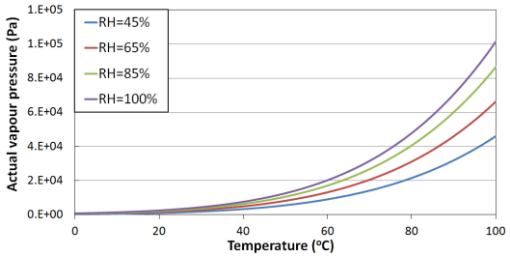

Fig. 8 Actual water vapour pressure versus temperature

Substituting Eq(5) and (6) into Eq(4), the relative humidity at the surface of back-sheet can be written as:

$$RH_m = \frac{P_w}{P_s(T_m)} = \frac{RH_a \cdot f(T_a) \cdot P_s'(T_a)}{f(T_m) \cdot P_s'(T_m)} \tag{7}$$

where $P_s'(T_a)$ and $P_s'(T_m)$ are saturated water vapour pressure of pure water at ambient temperature T_a and module temperature T_m, $f(T_a)$ and $f(T_m)$ are relative enhancement factor at T_a and T_m. For outdoor exposure, module temperature is often different from ambient temperate due to irradiance, wind speed, installation method, heat exchange with the ambient and the condition of the sky etc. As pointed out above, in laboratory based damp-heat tests, T_a equals T_m, i.e. relative surface humidity of back-sheet simply becomes ambient relative humidity:

$$RH_m = RH_a \tag{8}$$

A humidity dose model can then be established to quantify the effective cumulative stresses imposed on the module that contribute to the degradation process. In the following, assumptions are made that the loss of adhesion is a process depending on module micro-climatic conditions and is independent of the state of the module.

The latter clearly is a simplification, as in reality modules will oscillate between drying out and absorbing humidity. However, in the case of laboratory, the steady state experiments simplify understanding and will give a good insight into the effects of humidity on adhesion. The micro climatic relative surface humidity of back-sheet (RH_m) is considered as the dominating driving factor while module temperature is an accelerating factor which can be modeled using an Arrhenius function. The Arrhenius form is a commonly used acceleration model defining the relationship between degradation and temperature when a single mechanism dominates the ageing process [24-27]. This allows the development of a model to predict device behaviour in different operating environments. A cumulative function of time with relative surface humidity of back-sheet and module temperature as weighting factors within time duration of Δt can be established as following:

$$dose = RH_m \cdot e^{-\frac{Ea}{RT_m}} \cdot \Delta t \quad (9)$$

where E_a is the activation energy of the degradation process, R is the gas constant (8.314J/(K mol)) or Boltzmann's constant (8.617 x 10-5 ev/K) depending on the unit and T_m is the absolute module temperature in Kelvin. Considering the postulated RH_m in Eq (7) and (8), the humidity dose for the tests in this study can be written as:

$$dose = RH_m e^{-\frac{Ea}{RT_m}} \Delta t = \frac{RH_a f(T_a) P_s'(T_a)}{f(T_m) P_s'(T_m)} e^{-\frac{Ea}{RT_m}} \Delta t = RH_a e^{-\frac{Ea}{RT_m}} \Delta t \quad (10)$$

This model implies that it is not the ambient humidity but the relative surface humidity of back-sheet the most important driving factor for moisture ingress. It considers the influences of module temperature on micro climatic humidity. However, this dose model is only responsible for degradation induced by humidity and may only apply to limited temperature and humidity levels. The key descriptor required for the prediction of ageing is the activation energy which is determined in the next section.

4.2 Adhesion degradation and humidity dose & Activation energy

It is believed that the degradation of adhesion strength increases with the increasing of humidity dose, but in which form whether it is linear, exponential, power or logarithmic is unknown. Here we investigated two different approaches, i.e. conventional linear and an exponential degradation models. For each scenario, the activation energy is calculated and the relationship between adhesion degradation and humidity dose is discussed.

(a) Linear Model

Linear degradation model assumes the adhesion strength degradation (ΔS) to be proportional to humidity dose:

$$\Delta S = k \cdot dose = k \cdot RH_a \cdot e^{-\frac{Ea}{RT_m}} \cdot \Delta t \quad (11)$$

$$R_D = \frac{\Delta S}{\Delta t} = k \cdot RH_a \cdot e^{-\frac{Ea}{RT_m}} \quad (12)$$

This enables the extraction of E_a by taking the natural logarithm of degradation rate (R_D) and reciprocal of T_m which will generate an Arrhenius plot:

$$\ln \frac{\Delta S}{\Delta t} = -\frac{Ea}{R}\frac{1}{T_m} + \ln(k \cdot RH_a) \quad (13)$$

Fig. 9 shows the Arrhenius plot results for this study at constant RH_a of 85% but varying T_m of 95°C, 85°C and 65°C. Average R_D at each of the three testing conditions was used to get the plot. A linear relationship is observable and its slope allows the determination of E_a:

$$slope = -\frac{Ea}{R} = -6466 \quad (14)$$

$$Ea = 54kJ/mol = 0.56eV \quad (15)$$

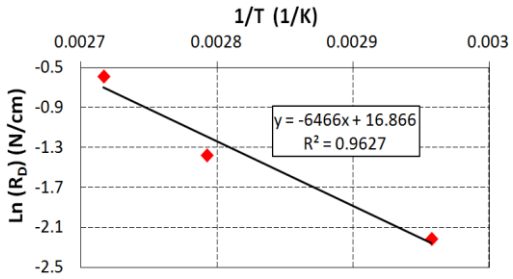

Fig. 9 Arrhenius plot between natural logarithm of degradation rates and the inverse of absolute module temperature

With the activation energy calculated, the proposed humidity dose in Eq(10) can be computed for all the five humidity and temperature conditions listed in Table 1. The adhesion strength degradation shown in Fig. 6 can then be re-investigated as dependent on the humidity dose with the results plotted in Fig. 10. According to the defined linear degradation model in Eq(11), adhesion strength after a certain time degradation (S) should be:

$$S = S_0 - \Delta S = S_0 - k \cdot dose \quad (16)$$

However, it is seen from Fig. 10 that the adhesion strength does not follow the linear approximation but shows a good exponential decay. This implies that the linear form does not suit the degradation well and an exponential model may better represent the degradation which is illustrated in scenario (b). The divergences between the proposed model and the experimental data may be resulted from the assumption that constant degradation exist throughout the whole ageing procedure which in reality is a slowing down process. The usage of average R_D hided the decreasing features of degradation.

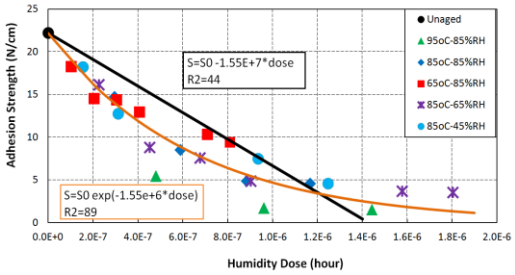

Fig. 10 Degradation of adhesion strength versus humidity dose using activation energy calculated from linear model

(b) Exponential Model

By the enlightenment of Fig.10, an exponential model can be established to describe the correlation between adhesion strength and humidity dose during degradation:

$$S = S_0 e^{-k \cdot dose} = S_0 e^{-k \cdot RH_a \cdot e^{-\frac{Ea}{RT_m}} \cdot \Delta t} \quad (17)$$

Eq (17) can be restructured into the following form by removing S_0 to the left side of the equation and then taking the natural logarithm of both sides twice:

$$\ln(-\ln(\frac{S}{S_0})) = -\frac{Ea}{RT_m} + \ln(k \cdot RH_a \cdot \Delta t) \quad (18)$$

By plotting $\ln(-\ln(S/S_0))$ vs. $1/T_m$, straight lines can be obtained with E_a/R determines the slope of the curve and the combined parameter of $(k*RH_a*\Delta t)$ determines the intercept. In principle, at constant RH_a but varying T_m, parallel lines with the same slope but different intercepts can be obtained at different degradation times. Fig. 11 shows such curves at RH_a of 85% but varying temperatures of 95°C, 85°C and 65°C at degradation times of 24h, 48h and 72h respectively. The three data sets can all be fitted with linear curves and are almost parallel with each other indicating a similar slope. Taking the average slope of the three fitted curves gives us an activation energy of 63kJ/mol (0.65eV).

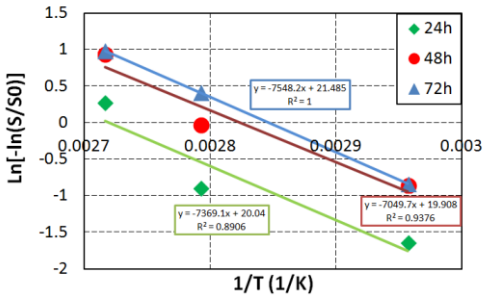

Fig. 11 Plot of $\ln(-\ln(S/S_0))$ against inverse of absolute module temperature at degradation times of 24h, 48h and 72h for exposures at 95°C/85%RH, 85°C/85%RH, 65°C/85%RH

Like what has been done for the linear model, the adhesion strength vs. humidity dose is also investigated for the exponential model with the results shown in Fig. 12. The five curves in Fig. 6 have normalised into one curve and a strong exponential agreement between adhesion strength and humidity dose is evident which can be approximated as:

$$S = S_0 e^{-3.28*10^7 \cdot dose} \qquad (19)$$

The fitted coefficient of determination is over 0.92 which means highly correlated. This verifies the suitability of exponential model to describe the correlation between adhesion strength and humidity dose.

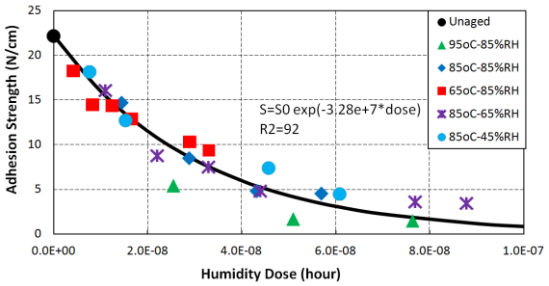

Fig. 12 Degradation of adhesion strength versus humidity dose with activation energy calculated from exponential model

The degradation may be caused by multiple mechanisms and may follow Eq (10) and (19) over only limited temperature and humidity ranges. In Fig. 12, data at 95°C/85%RH show some divergences from the fitting which indicates that some other degradation mechanisms may have been triggered or are becoming increasingly important at this high temperature which slightly deviate these data from the fitting. 95°C is much higher than the melting point of EVA which is around 40°C - 60°C so that the polymer may have experienced structural and morphology changes resulting in different degradation mechanisms. But the data at 95°C/85%RH in Fig. 12 are not too far away from the other four conditions which mean the primary degradation mechanism is still humidity effects.

Therefore, the adhesion strength along with cumulative stresses experienced by PV module within a certain damp heat degradation period can be modelled by an exponential function through the proposed humidity dose. Many other issues like degradation induced by other stress factors and the response to the cyclic environmental changes etc. need to be solved before an outdoor prediction can be made but these are out the scope of this research.

5 CONCLUSIONS

The durability of adhesion between back-sheet and encapsulant for commercial crystalline silicone mini-modules to withstand the effects of humidity ingress has been investigated under humid conditions. This was achieved by exposing the devices at different stress levels of humidity and at different temperatures. It is shown that the loss of adhesion varied significantly under the different regimes. Under these conditions, humidity is the primary driver of the reduction of adhesion strength and temperature determines the speed of degradation. Linking this particular stress mechanism to operating environments can be done by developing a stress dose model to describe the cumulative stresses imposed on PV modules and investigate the relationship between degradation and the dose. In this research, a humidity dose is defined by assuming the relative surface humidity at the back sheet as the main driving factor and module temperature as the accelerant with an Arrhenius influence of the degradation process. The calculation of relative surface humidity of back-sheet transfers the environmental humidity to module surface humidity and considers the contribution of module temperature on the humidity at the surface of back-sheet. This approach enables modelling of the loss of adhesion due to humidity with a single set of variable.

This is the first step of modelling the realistic loss of adhesion in outdoor operation, where devices not only experience humidity but also varying humidity, cyclic temperature and photochemical reactions etc. Further work will be needed to quantify additional effects from the other stresses of thermal, thermal cycling, irradiance including UV and the combination of these factors before developing a full model but this can only be achieved on a mechanism-by-mechanism level and built of an effective superimposing model. The link between adhesion strength or, more generally, encapsulant state and actual device performance and safety are still a goal which requires significant additional amounts of work.

References

[1] J. Pern, APP International PV Reliability Workshop, Shanghai, China, (2008).
[2] J.A. del Cueto, T.J. McMahon, Progress in Photovoltaics Research and Applications 10 (2002)15-28.
[3] P. Sanchez-Friera, M. Piliougine, J. Pelaez, J.

Carretero, M. Sidrach de Cardona. Progress in Photovoltaics Research and Applications 19 (2011) 658–666.
[4] D. Polverini, M. Field, E. Dunlop, W. Zaaiman, Progress in Photovoltaics Research and Applications 21 (2012) 1004–1015.
[5] C.E. Chamberlin, M.A. Rocheleau. et al, 37th IEEE PV Specialists Conference, Seattle, WA, (2011).
[6] M. Saly, M. Ruzinsky, P. Redi, 17th EUPVSEC, Munich, Germany, (2001).
[7] K.R. McIntosh, N.E. Powell, A.W. Norris, J.N. Cotsell, B.M. Ketola, Progress in Photovoltaics Research and Applications (2010).
[8] M.A. Quintana, D.L. King, T.J. McMahon, C.R. Osterwald, 29th IEEE PVSEC, New Orleans, USA, (2002).
[9] IEC 61215, 2005.
[10] IEC 61646, 2008.
[11] M. Kempe, 37th IEEE Photovoltaic Specialists Conference, Seattle, Washington, (2011).
[12] T.P. Ferguson, J. Qu, IEEE International Symposium on Advanced Packaging Materials: Processes, Properties and Interfaces 19 (2005) 294-300.
[13]. MD. Kempe, Solar Energy Materials & Solar Cells 90 (2006) 2720–2738.
[14] J. Kapur, K. Proost, CA. Smith, 34th IEEE Photovoltaic Specialists Conference, Philadelphia, PA, USA, (2009).
[15] TJ. McMahon, G. Jorgensen, Proceedings of the 4th World Conference on PV Energy Conversion, (2006) 2062-2065.
[16] FJ. Pern, SH. Glick, National Center for Photovoltaics and Solar Program Review Meeting, Denver, Colorado, (2003).
[17] FJ. Pern, GJ. Jorgensen, 31st IEEE Photovoltaics Specialists Conference and Exhibition, Lake Buena Vista, Florida (2005).
[18] BS EN 28510-1:1993, ISO8510-1:1990, (1993).
[19] M. Koehl, M. Heck, S. Wiesmeier, J. Wirth, Solar Energy Materials & Solar Cells 95 (2011) 1638–1646.
[20] MC. Alonso Garcia, JL. Balenzategui, Renewable Energy 29 (2004) 1997–2010.
[21] D.L. King, W.E. Boyson, J.A. Kratochvil, Sandia National Laboratory, Department of Energy, (2004).
[22] M. Koehl, M. Heck, S. Wiesmeier, Solar Energy Materials & Solar Cells 99 (2012) 282-291.
[23] BS 1339-1:2002, (2002).
[24] S. Kurtz et al. Progress in Photovoltaics Research and Applications 19 (2011) 954–965.
[25] N. Gorjian, L. Ma, M. Mittinty, P. Yarlagadda and Y. Sun, 4th World Congress on Engineering Asset Management, Athens, Greece, (2009).
[26] M. Koehl, PV Module Reliability Workshop, Berlin, Germany, (2011).
[27] D.C.C. Lam, F. Yang, P. Tong, IEEE Transaction on components and packaging technology 22 (1999) 44-48.